TẠP CHÍ KHOA HỌC
TRƯỜNG ĐẠI HỌC QUY NHƠN

Ảnh hưởng của tỷ lệ mol giữa ion kim loại/axit citric và nhiệt độ nung đến cấu trúc và hoạt tính quang xúc tác của $YFeO_3$

Dương Đức Lương, Nguyễn Văn Thắng*

Khoa Khoa học Tự nhiên, Trường Đại học Quy Nhơn, Việt Nam

Ngày nhận bài: 11/03/2020; Ngày nhận đăng: 15/04/2020

TÓM TẮT

Vật liệu $FeYO_3$ tổng hợp thành công bằng phương pháp sol-gel đã được khảo sát đặc trưng bằng phương pháp nhiễu xạ tia X, kính hiển vi điện tử quét, phương pháp phổ hồng ngoại, phương pháp phổ phản xạ khuếch tán tử ngoại khả kiến. Ảnh hưởng của điều kiện tổng hợp vật liệu như tỷ lệ mol giữa kim loại/axit citric, nhiệt độ nung đến cấu trúc và hoạt tính quang xúc tác của $FeYO_3$ đã được khảo sát một cách có hệ thống. Kết quả thực nghiệm cho thấy, tất cả các vật liệu $YFeO_3$ thu được có hoạt tính quang xúc tác trong vùng ánh sáng khả kiến thông qua sự phân hủy xanh metylen trong dung dịch nước. Cụ thể, vật liệu $YFeO_3$ được thiêu kết ở 900 ^oC ứng với tỷ lệ mol 1:2 của kim loại và axit citric cho hiệu suất quang xúc tác tốt nhất so với các vật liệu $YFeO_3$ được tổng hợp trong cùng điều kiện nhưng được nung ở nhiệt độ khác.

Từ khóa: *$YFeO_3$, phương pháp sol-gel, quang xúc tác, ánh sáng nhìn thấy và xanh methylen.*

*Tác giả liên hệ chính.
Email: nguyenvanthang@qnu.edu.vn

JOURNAL OF SCIENCE
QUY NHON UNIVERSITY

Influence of molar ratio of metal ions to citric acid and annealing temperature on structure and photocatalytic properties of $YFeO_3$ photocatalysts synthesized by sol-gel method

Duong Duc Luong, Nguyen Van Thang*

Faculty of Natural Sciences, Quy Nhon University, Vietnam

Received: 11/03/2020; Accepted: 15/04/2020

ABSTRACT

$YFeO_3$ materials, which were successfully synthesized by the sol-gel method, were characterized by X-ray diffraction (XRD), Scanning Electron Microscopy (SEM), Fourier Transform Infrared Spectroscopy (FT-IR), and Ultraviolet-Visible Diffuse Reflectance Spectroscopy (UV-Vis DRS). The influence of the synthesizing conditions such as the molar ratio of metal ions to citric acid, and the annealing temperature on the structure and photocatalytic properties of $YFeO_3$ samples has been systematically investigated. The experimental results show that all obtained $YFeO_3$ samples exhibit photocatalytic activities under the visible light region through the photodegradation of methylene blue (MB) in an aqueous solution. Specifically, the $YFeO_3$ sample, which was synthesized with the molar ratio of 1: 2 metal ions/citric acid and annealed at 900 ^oC, shows the highest photocatalytic degradation efficiency compared to $YFeO_3$ samples synthesized under the same conditions but annealed at other temperatures.

Keywords: *$YFeO_3$ photocatalysts, sol-gel method, photocatalysis, visible-light irradiation, and methylene blue degradation.*

1. INTRODUCTION

Environmental concerns, especially water pollution, have been a leading challenge for humanity over the years due to the population and economic growth. Many different methods of treating contaminated water have been reported.[1] However, these methods have proved ineffective because they do not completely remove pollutants or are time-consuming and costly in operation. Therefore, the search for new and more effective water treatment methods is essential.

Recently, a method that has been researched and applied by scientists in the treatment of polluted water is the use of photocatalytic materials in order to decompose toxic organic compounds in water.[2] Among various photocatalysts, TiO_2-based catalysts have been extensively studied owing to its high physical and chemical stability, low production cost and high photocatalytic activity under irradiation of UV light.[3–7] Due to the wide band gap (Eg) (≈ 3.2 eV), however, TiO_2 is limited in its application under visible light.[8] Hence, it is less effective when used as photocatalysts in the visible light region. Visible light is a source of 43% of the sun's energy spectrum, a source of clean energy and is considered endless. Thus, it is highly desirable to look for photocatalysts with a narrow band gap so that they have high photocatalytic activity under the visible light irradiation.

*Corresponding author.
Email: nguyenvanthang@qnu.edu.vn

In the search for new materials over the years, iron-based (III) semiconductors such as Fe_2O_3, $FeBiO_3$ and especially $YFeO_3$ become more and more attractive since they have a narrow band gap and thus effectively operating under the irradiation of visible light.[8,9] However, $YFeO_3$ is thermodynamically unstable and can be converted to a more stable form Fe_3O_4 or $Y_3Fe_5O_{12}$ at high temperatures, so it is difficult to synthesize pure $YFeO_3$.[10] On the other hand, most current methods for synthesizing $YFeO_3$ require high-temperature annealing, resulting in a high-energy consumption and the creation of large particle size materials. Therefore, it is highly desirable to optimize the synthesizing conditions for $YFeO_3$.

This work focuses on the fabrication of $YFeO_3$ photocatalysts by the sol-gel method. The influence of both the molar ratio of metal ions to citric acid and the annealing temperature on the crystal structure, surface morphology, and methylene blue (MB) photodegradation efficiency of obtained $YFeO_3$ materials was systematically investigated.

2. EXPERIMENT

2.1. Chemicals

The chemicals used in our experiments were yttrium oxide (Y_2O_3, 99.99% purity), citric acid ($C_6H_8O_7$, 98% purity), iron(III) nitrate nonahydrate ($Fe(NO_3)_3.9H_2O$, 98%), methylene blue ($C_{16}H_{18}N_3SCl$) and nitric acid (HNO_3, 65%).

2.2. Synthesis of $YFeO_3$ by the sol-gel method

In order to prepare $YFeO_3$ samples by the sol-gel method, 3.513 g of Y_2O_3 and 12.560g of $Fe(NO_3)_3.9H_2O$ were dissolved in 100 mL of HNO_3 1 M in a 250 mL glass beaker by magnetically stirring constantly at room temperature. When the mixture became transparent, different amounts of citric acid was added and continuously stirred for 24 hours. After that, the temperature was increased to 80ºC and constantly stirred for 2 hours to create the sol. In order to obtain the gel, the temperature was raised to 100 ºC to remove water molecules from the sol. When the water evaporates, the sol changes into a highly viscous gel. The obtained gel was dried in an oven at 200 ºC for a period of 2 hours. At this temperature, the gel burns and releases NO_2 gas from the gel layer, causing a significant increase in the gel volume. As a result, a yellow-brown powder called a dry gel was obtained. The powder was then annealed at various temperatures between 700 to 1000 ºC for 5 hours in the air to obtain the final products. The resultant samples were denoted as $YFeO_3$.850.(1:n) (n = 1, 2, 3 and 4) and $YFeO_3$.T(1:2) (T = 700, 800, 900 and 1000) for samples annealed at 850 ºC with different molar ratios of metal ions to citric acid and samples annealed at different temperatures, respectively.

2.3. Material characterizations

XRD patterns of obtained samples were collected at room temperature by means of a D8 Advance Brucker diffractometer operated at 40 kV and 100 mA with Cu-Kα radiation ($\lambda_{K\alpha}$ = 1,5406 Å) in a 2θ range between 20º and 80º at the step of 0.03º. FT-IR spectra of obtained samples were recorded by means of an IRAffinity-1S in the spectra range of 4000 to 400 cm^{-1}. The optical properties of obtained $YFeO_3$ photocatalysts were investigated by UV-Vis DRS using a UV-Vis spectrometer Jasco-V670. The particle size and surface morphology of the samples were investigated by SEM carried out on Nano SEM-450.

2.4. Photocatalytic activities of $YFeO_3$

Photocatalytic activities of the obtained $YFeO_3$ samples were evaluated through the photodegradation of MB in an aqueous solution under the visible light irradiation. Typically, 0.1 g of the photocatalyst was added to 80 mL of MB solution (concentration of 10 mg/L) in a 250 mL glass beaker. After that, the mixture was continuously stirred in the dark for 2 hours in order to allow the adsorption and desorption processes of MB molecules on the surface of the photocatalyst to reach the equilibrium before investigating its photocatalytic activities under the irradiation of a tungsten filament

lamp 60 W – 220 V in a period of 6 hours. At certain irradiation intervals, 7 mL of the mixed suspension was taken out and centrifuged to remove the photocatalyst from the mixture (6000 rpm, 20-minute centrifugation time). The residual MB concentration as a function of the irradiation time was analyzed by collecting variation of the absorbance at 663 nm using UV-Vis CE-2011 spectrometer. MB photodegradation efficiency is calculated by the following formula:

$$H = \frac{C_o - C}{C_o}.100$$

In which, C_o is the initial concentration of MB and C is the remaining concentration of MB after each corresponding irradiation time.

3. RESULTS AND DISCUSSION

3.1. Effect of the molar ratio of metal ions to citric acid on the crystal structure, surface morphology, and methylene blue decomposition efficiency

With the aim to optimize the lattice crystal structure of $YFeO_3$ materials, different molar ratios of metal ions to citric acid (1:1, 1:2, 1:3 and 1:4) were employed during the sample synthesis.

3.1.1. Effect of the molar ratio of metal ions to citric acid on the crystal structure

The structure of the obtained $YFeO_3$.850(1:n) samples was investigated by both XRD and FT-IR. Figure 3.1 shows the XRD patterns collected at room temperature for the $YFeO_3$.850(1:n) samples.

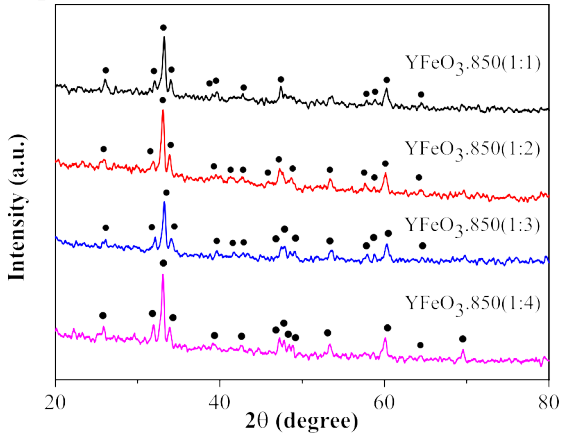

Figure 3.1. XRD patterns for $YFeO_3$.850(1:n) samples.

As can be clearly seen in Figure 3.1, the diffraction peaks of the $YFeO_3$.850(1:n) samples are completely consistent with the JCPDS Card No.39-1489. This indicates that all $YFeO_3$.850(1:n) samples crystallize in the orthorhombic structure (space group Pnma(62)) with deformed perovskite structure [11] and have the lattice parameters a = 0,5588 nm, b = 0,7595nm, c = 0,5274 nm. The main diffraction peaks are at 2θ = 25.9, 31.9, 33.1, 33.9, 47.3, 53.4 and 60.2° which correspond to the crystal planes of (111), (200), (121), (002), (040), (311) and (042), respectively. The intensity of diffraction peaks is relatively high, indicating that the obtained materials have high crystallinity. The position and intensity of all diffraction peaks do not change much, suggesting that the molar ratio of metal ions to citric acid hardly changes the crystal structure of the synthetic materials.

Table 3.1. Variation of average crystallite size for $YFeO_3$.850(1:n) samples

Sample	*$YFeO_3$.850(1:n)*			
	1:1	*1:2*	*1:3*	*1:4*
Average crystallite size (nm)	19.322	17.058	16.657	17.148

The average crystallite size of $YFeO_3$ samples was calculated by applying the Debye - Scherrer formula to the max intensity peak (121), which was fitted with the OriginPro 8.5.1 software to identify the peak position and the full-width-at-half-maximum. The results obtained in Table 3.1 show that all samples have small crystallite size (< 20 nm), in which the sample corresponding to a molar ratio of 1:1 between the number of metal ions and citric acid has the largest crystallite size.

The FT-IR spectra of $YFeO_3$ samples after annealing at 850 °C for 5 hours shown in Figure 3.2 consist of four main absorption regions: the first one corresponds to a broad absorption band at 3700 - 3200 cm^{-1} due to the O-H stretching of the free moisture in the air [12]; the second region corresponds to peaks at 2353 cm^{-1} due to the oscillation of the C = O group of CO_2 present in

the air [13]; the third region corresponds to a wide absorption band at 1572 - 1385 cm^{-1} which may be attributed to the stretching of C-O bonds [14]; the fourth region corresponds to the characteristic absorption band at 568 cm^{-1} due to the Fe-O stretching mode of the ortho-ferrite systems [14,15]. When changing the molar ratio of metal ions to citric acid, there are no additional peaks on the FT-IR spectra, indicating that the change in the molar ratio of metal ions and citric acid hardly affects the lattice crystal structure of obtained $YFeO_3$ samples. This is in a good agreement with the XRD analysis.

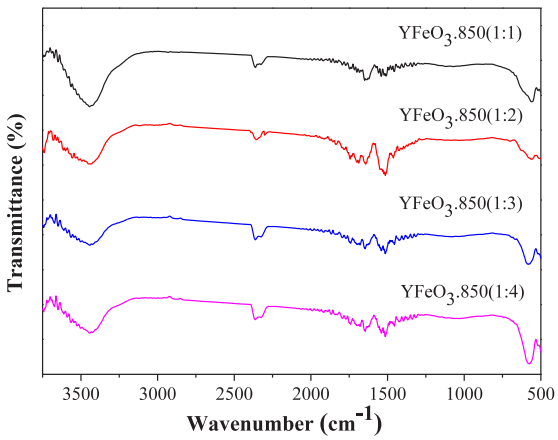

Figure 3.2. FT-IR spectra of $YFeO_3$.850(1:n) samples

3.1.2. Effect of the molar ratio of metal ions to citric acid on the surface morphology

SEM has been used to investigate the effect of the molar ratio of metal ions to citric acid on the surface morphology of $YFeO_3$ samples. The SEM images of the $YFeO_3$ samples synthesized by the sol-gel method and annealed at 850 °C for 5 hours with different molar ratios of metal ions to citric acid in Figure 3.3 show that the particle size of all samples was at the nanoscale. Moreover, for the samples with the molar ratios of 1:3 and 1:4 between metal ions and citric acid, the particles are more uniform and have less cohesion than samples with the molar ratios of 1:1 and 1:2 between metal ions and citric acid. It is worth noting that the crystallite size calculated by XRD is the smallest – mostly like a single crystal in powder form. Since particle may be present as a single crystal or an agglomeration of several crystals, the particle size determined by SEM is always larger than the crystallite size.

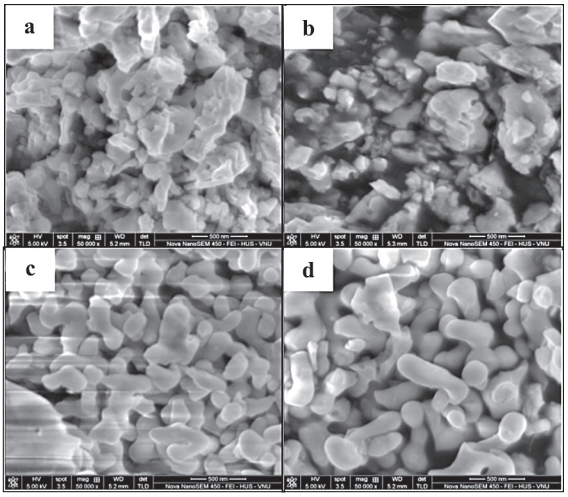

Figure 3.3. SEM images of $YFeO_3$.850(1:1) (a); $YFeO_3$.850(1:2) (b); $YFeO_3$.850(1:3) (c); $YFeO_3$.850(1:4) (d)

3.1.3. Effect of the molar ratio of metal ions to citric acid on the methylene blue photodegradation efficiency

In order to study the effect of the molar ratio of metal ions to citric acid on the MB photodegradation efficiency, the C/C_o versus the irradiation time is plotted and shown in Figure 3.4. In which, C_o is the concentration of MB solution after stirring 2 hours in the dark and C is the concentration of MB solution after irradiation time t (h). The results show that the sample corresponding to the molar ratio of 1:2 between metal ions and citric acid had a faster decrease in the concentration of MB than other samples synthesized under the same conditions but with different molar ratios of the metal ions to citric acid.

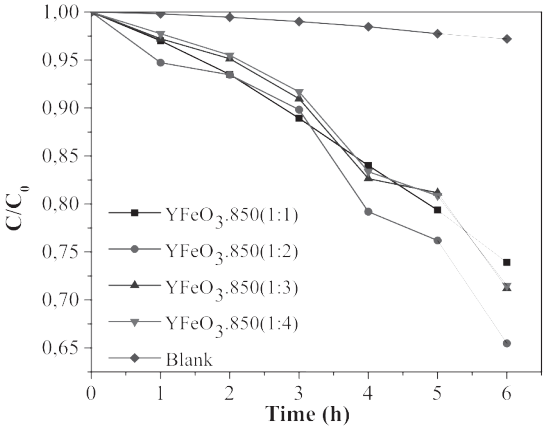

Figure 3.4. The C/C_o of MB as a function of the irradiation time for the blank and $YFeO_3$.850(1:n) samples

Table 3.2 shows the MB photodegradation efficiency with and without the presence of $YFeO_3$.850(1:n) samples after 6 hours of irradiation. In general, all samples have relatively low photodegradation efficiency. After 6 hours of irradiation, $YFeO_3$.850(1:2) sample has the highest decomposition efficiency (34.53%). Meanwhile, MB decomposition efficiency for $YFeO_3$.850(1:1), $YFeO_3$.850(1:3) and $YFeO_3$.850(1:4) samples are 26.09, 28.81 and 28.50%, respectively. Besides, for the blank sample, MB photodegradation efficiency is only 2.79%, suggesting that without the presence of $YFeO_3$ MB was hardly decomposed under irradiation conditions. Therefore, it can be concluded that the presence of $YFeO_3$ photocatalysts plays a vital role in the photodegradation of MB.

Table 3.2. MB photodegradation efficiency (%) for blank and $YFeO_3$.850(1:n) after 6 hours of irradiation

Sample	Photodegradation efficiency (%)
$YFeO_3$.850(1:1)	26.09
$YFeO_3$.850(1:2)	34.53
$YFeO_3$.850(1:3)	28.81
$YFeO_3$.850(1:4)	28.50
Blank	2.79

3.2. Effect of the annealing temperature on the lattice crystal structure, band gap energy and methylene blue photodegradation efficiency of $YFeO_3$

3.2.1. Effect of the annealing temperature on the lattice crystal structure of $YFeO_3$

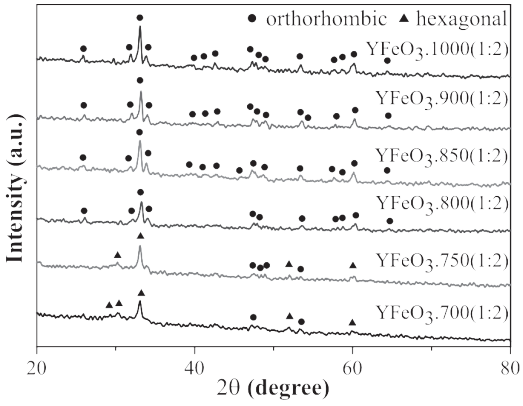

Figure 3.4. XRD patterns collected at room temperature for $YFeO_3$.T(1:2) samples

The XRD patterns measured at room temperature for $YFeO_3$.T(1:2) samples annealed at different annealing temperatures (700 - 1000°C) are shown in Figure 3.4. The experimental results show that samples annealed below 800 °C have the presence of both orthorhombic and hexagonal phases. However, when sintered at higher temperatures (800 - 1000 °C), the samples obtained have an orthorhombic single-phase structure. This can be explained by the fact that at high temperature the hexagonal structure phase (space group (P63/mmc)) will change to the orthorhombic phase that is thermodynamically stable.[16] Moreover, the diffraction peak corresponding to the highest intensity at $2\theta \approx 33.1°$ becomes sharper and has a higher intensity for increasing annealing temperature, indicating that the obtained samples have a better crystallinity and a larger crystallite size.

Table 3.3 presents the average crystallite size of $YFeO_3$ samples annealed at different temperatures, which was calculated by applying the Debye - Scherrer formula to the max intensity peak (121) at $2\theta \approx 33$. In general, the average crystallite size of all samples increases with increasing annealing temperature, especially for the sample annealed at 1000 °C.

Table 3.3. Variation of average crystallite size for $YFeO_3$.T(1:2) samples

Sample	Average crystallite size (nm)
$YFeO_3$.700(1:2)	12.850
$YFeO_3$.750(1:2)	16.524
$YFeO_3$.800(1:2)	15.436
$YFeO_3$.850(1:2)	17.058
$YFeO_3$.900(1:2)	16.627
$YFeO_3$.1000(1:2)	24.128

FT-IR spectra of $YFeO_3$.T(1:2) samples shown in Figure 3.5 include 4 main absorption regions like $YFeO_3$ samples sintered at 850°C as described in 3.1.1. However, the peak intensity absorbed at 568 cm^{-1} due to the asymmetric elongation of the Fe-O-Fe bond in the FeO_6 octahedron increases for increasing

the annealing temperature. This proves that the purity of the $YFeO_3$.T(1:2) samples is enhanced as the annealing temperature increases.

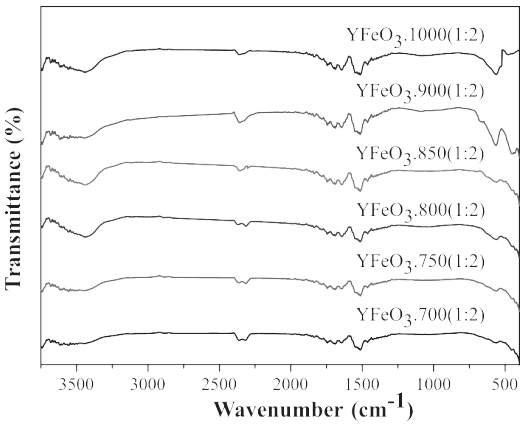

Figure 3.5. FT-IR spectra of $YFeO_3$.T(1:2) annealed at different temperatures

3.2.2. Effect of the annealing temperature on the band gap energy

UV-Vis DRS was used to investigate the effect of the annealing temperature on the band gap energy of obtained $YFeO_3$.T(1:2) samples. UV-Vis DRS spectra of these samples are shown in Figure 3.6.

The experimental results show that $YFeO_3$.T(1:2) samples annealed at different temperatures are active in the visible light region and the absorption band extends from the ultraviolet to the visible. On the other hand, when the annealing temperature increases, the light absorption region of the material shifts to the shorter wavelength region. This is in good agreement with the change in the color of obtained samples as a function of the annealing temperature.

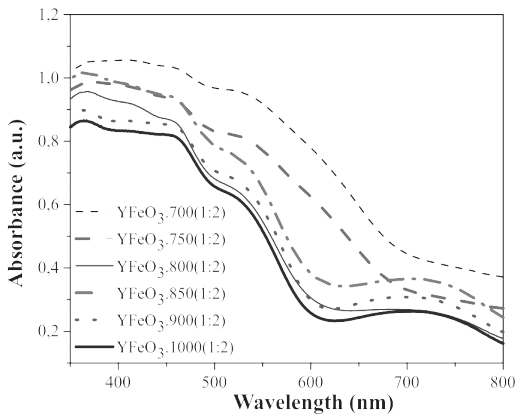

Figure 3.6. UV-Vis diffuse absorption spectra of the $YFeO_3$.T(1:2) samples

Since $YFeO_3$ is an indirect band gap semiconductor, the Kubelka-Munk function $[F(R)hv]^2$ versus the phonon energy was plotted to estimate the band gap energy of all samples. The results presented in Figure 3.7 and Table 3.4 show that the band gap energy increases in the annealing temperature range of 700 - 800 ºC and hardly changes as further increasing the annealing temperature to 1000 ºC.

Table 3.4. Variation in the band gap energy for $YFeO_3$.T(1:2) samples

Sample	E_g *(eV)*
$YFeO_3$.700(1:2)	2.25
$YFeO_3$.750(1:2)	2.36
$YFeO_3$.800(1:2)	2.48
$YFeO_3$.850(1:2)	2.43
$YFeO_3$.900(1:2)	2.43
$YFeO_3$.1000(1:2)	2.45

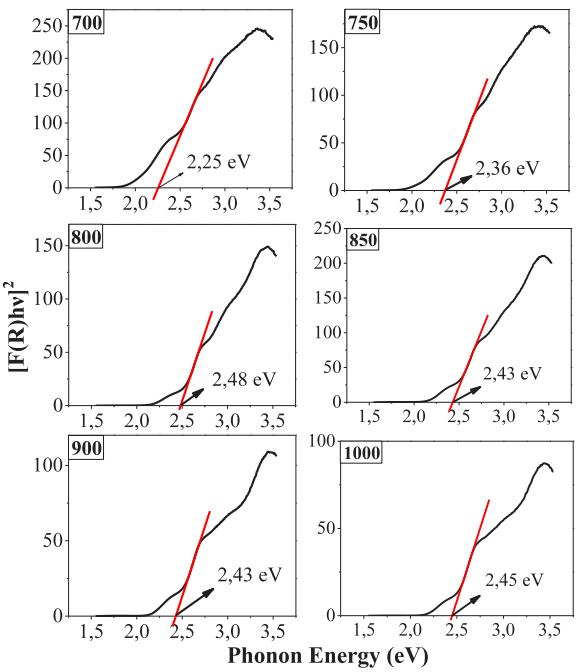

Figure 3.7. Plots of $[F(R)hv]^2$ versus phonon energy for $YFeO_3$.T(1:2) samples

3.2.3. Effect of the annealing temperature on the methylene blue photodegradation efficiency

Table 3.5. MB photodegradation efficiency (%) of $YFeO_3$ samples after a period of six-hour irradiation

Sample	Photodegradation efficiency (%)
$YFeO_3$.700(1:2)	36.94
$YFeO_3$.750(1:2)	27.40
$YFeO_3$.800(1:2)	28.50
$YFeO_3$.850(1:2)	34.53
$YFeO_3$.900(1:2)	48.99
$YFeO_3$.1000(1:2)	35.33

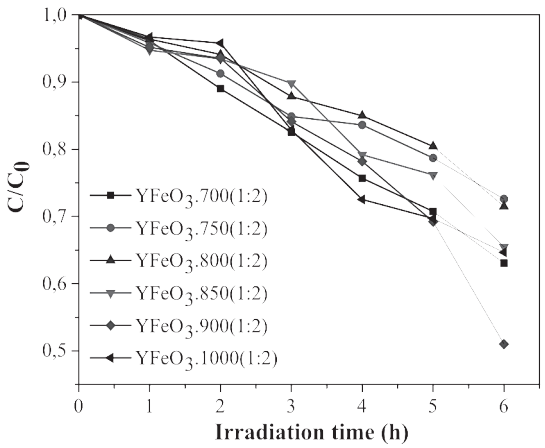

Figure 3.8. Kinetic of the photocatalytic degradation of MB for $YFeO_3$.T(1:2) samples under visible light irradiation

The photocatalytic activity survey results presented in Table 3.5 indicate that the $YFeO_3$ sample synthesized with a molar ratio of 1:2 metal ions/citric acid and annealed at 900 ºC has the highest MB photodegradation efficiency (48.99% after 6 hours of irradiation). Meanwhile, MB decomposition efficiency for $YFeO_3$ samples synthesized under the same conditions but annealed at 700, 750, 800, 850 and 1000ºC was 36.94, 27.40, 28.50, 34.53 and 35.33%, respectively. This may be because the sample annealed at 900 ºC has higher crystallinity than those annealed at 700 - 850 ºC and has a smaller particle size than the samples annealed at 1000ºC.

3.3. Kinetic of photocatalytic reactions for $YFeO_3$

Table 3.6. Data obtained from the $YFeO_3$ samples when evaluating the kinetics of the photocatalytic reactions by employing the Langmuir-Hinshelwood model

Sample	Kinetic equation	K_{app} (h^{-1})	R^2
$YFeO_3$.850(1:1)	y = 0.05055x – 0.01988	0.05055	0.97979
$YFeO_3$.850(1:2)	y = 0.06685x – 0.03514	0.06685	0.91017
$YFeO_3$.850(1:3)	y = 0.05432x – 0.03275	0.05432	0.91637
$YFeO_3$.850(1:4)	y = 0.05434x – 0.03652	0.05434	0.91582
$YFeO_3$.700(1:2)	y = 0.0771x – 0.01988	0.0771	0.98619
$YFeO_3$.750(1:2)	y = 0.05149x – 0.00636	0.05149	0.98106
$YFeO_3$.800(1:2)	y = 0.05252x – 0.02283	0.05252	0.94071
$YFeO_3$.900(1:2)	y = 0.10124x – 0.07855	0.10124	0.84127

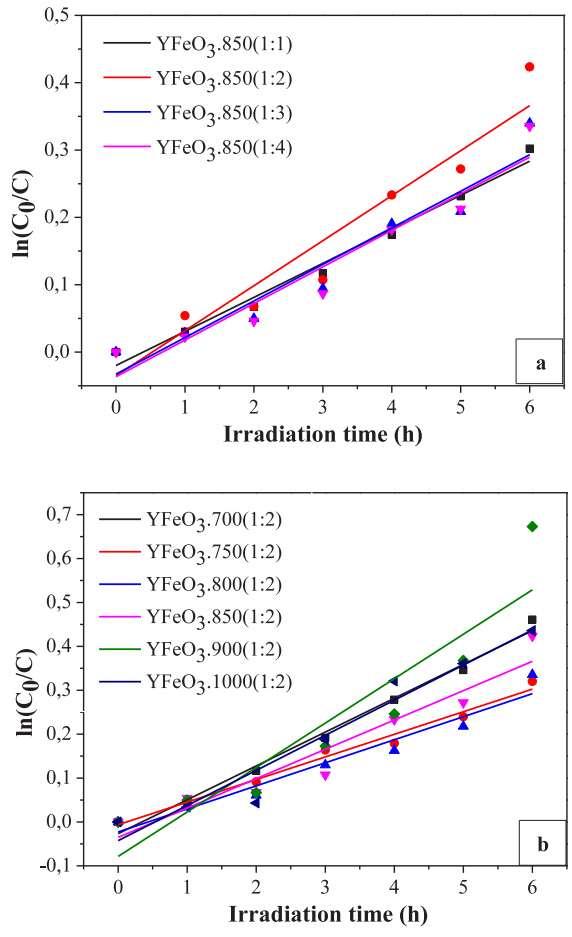

Figure 3.9. The plots of $\ln(C/C_o)$ versus irradiation time for the photocatalytic degradation of MB of $YFeO_3$.850(1:n) and $YFeO_3$.T(1:2) samples

The plots of $\ln(C_o/C)$ versus the irradiation time shown in Figure 3.9 is linear, revealing that the photocatalytic reactions of $YFeO_3$ materials for MB photodegradation follow the Langmuir-Hinhshelwood kinematic model with the high coefficient of determination.

The analysis results of MB photodegradation kinetics for the $YFeO_3$ samples presented in Table 3.9 show that the $YFeO_3$.900(1:2) sample shows the highest photodegradation rate ($k = 0.10124\ h^{-1}$), which is 1.5 times higher than that of $YFeO_3$.850(1:2) sample.

4. CONCLUSION

In this paper, we systematically investigated the effect of both the molar ratio of metal ions to citric acid and the annealing temperature on structure and photocatalytic properties of $YFeO_3$ samples that were fabricated by the sol-gel method. XRD analysis indicates that all $YFeO_3$ samples obtained mainly crystallize in the orthorhombic structure (space group Pnma (62)) with deformed perovskite structure. All $YFeO_3$ photocatalysts obtained were found to exhibit photocatalytic activities in the visible light region. In particular, the $YFeO_3$ sample annealed at 900 ^oC with a molar ratio of 1: 2 between metal ions and citric acid has the highest MB catalytic decomposition efficiency compared to $YFeO_3$ samples fabricated under the same condition but annealed at other temperatures.

ACKNOWLEDGEMENTS

This study is conducted within the framework of science and technology projects at institutional level of Quy Nhon University under the project code T2019.613.08.

REFERENCES

1. P. Rajasulochana and V. Preethy. Comparison on efficiency of various techniques in treatment of waste and sewage water – A comprehensive review, *Resource - Efficient Technologies,* **2016,** *2,* 175–184.
2. Suresh C. Ameta. Advanced Oxidation Processes for Wastewater Treatment, *Advanced Oxidation Processes for Wastewater Treatment: Emerging Green Chemical Technology*, **2018,** 1–12.
3. J. Zhang, Q. Xu, Z. Feng, M. Li, and C. Li. Importance of the Relationship between Surface Phases and Photocatalytic Activity of TiO_2, *Angewandte Chemie - International Edition*, **2008**, *47*(9), 1766–1769.
4. Q. Guo, C. Zhou, Z. Ma, and X. Yang. Fundamentals of TiO_2 Photocatalysis: Concepts, Mechanisms, and Challenges, *Advanced Materials,* **2019,** *31,* 1–26.
5. M. Pawar, S. T. Sendoğdular, P. Gouma. A brief overview of TiO_2 photocatalyst for organic dye remediation: Case study of reaction mechanisms involved in Ce-TiO_2 photocatalysts system, *Journal of Nanomaterials,* **2018**, *2018,* 1–13.
6. L. Zhao, X. Chen, X. Wang, Y. Zhang, W. Wei, Y. Sun, M. Antonietti, and M. M. Titirici.One-step solvothermal synthesis of a carbon@TiO_2 dyade structure effectively promoting visible-light photocatalysis, *Advanced Materials,* **2010**, *22*(30), 3317–3321.
7. S. C. Li and U. Diebold. Reactivity of TiO_2 rutile and anatase surfaces toward nitroaromatics, *Journal of the American Chemical Society,* **2010,** *132*(1), 64–66.
8. S. Sun, W. Wang, H. Xu, L. Zhou, M. Shang, and L. Zhang. $Bi_5FeTi_3O_{15}$ Hierarchical Microflowers: Hydrothermal Synthesis, Growth Mechanism, and Associated Visible-Light-Driven Photocatalysis, *Journal of Physical Chemistry C*, **2008**, *112*, 17835–17843.
9. X. Lu, J. Xie, H. Shua, J. Liu, C. Yin, J. Lin. Microwave-assisted synthesis of nanocrystalline $YFeO_3$ and study of its photoactivity, *Materials Science and Engineering B: Solid-State Materials for Advanced Technology*, **2017**, *138*(3), 289–292.
10. S. Mathur, M. Veith, R. Rapalaviciute, H. Shen, G. F. Goya, W. L. M. Filho, and T.S. Berquo. Molecule Derived Synthesis of Nanocrystalline

$YFeO_3$ and Investigations on Its Weak Ferromagnetic Behavior, *Nanoengineered Nanofibrous Materials,* **2004**, *169*(16), 425–442.

11. D. du Boulay, E. N. Maslen, V. A. Streltsov & N. Ishizawa. A synchrotron X-ray study of the electron density in $YFeO_3$, *Acta Crystallographica Section B Structural Science,* **1995**, *51*(6), 921–929.

12. M. C. Navarroa, E. V. Pannunzio-Minerb, S. Pagolab, M. InesGomeza, R. E. Carboniob. Structural refinement of $Nd[Fe(CN)_6].4H_2O$ and study of $NdFeO_3$ obtained by its oxidative thermal decomposition at very low temperatures, *Journal Solid State Chem,* **2005**, *178*(3), 847–854.

13. A. Gatelytė, D. Jasaitis, A. Beganskienė, A. Kareiva. Sol-gel synthesis and characterization of selected transition metal nano-ferrites, *Medziagotyra*, **2011**, *17*(3), 302–307.

14. N. T. Thuy, D. L Minh. Size Effect on the Structural and Magnetic Properties of Nanosized Perovskite $LaFeO_3$ Prepared by Different Methods, *Advances in Materials Science and Engineering,* **2012**, *2012*(3), 1–6.

15. Q. Lin, J. Xu, F. Yang, X. Yang and Y. He. The influence of Ca substitution on $LaFeO_3$ nanoparticles in terms of structural and magnetic properties, *Journal of Applied Biomaterials and Functional Materials,* **2018**, *16*(1S), 17–25.

16. J. Li, U. G. Singh, T. D. Schladt, J. K. Stalick, S. L. Scott, and R. Seshadri. Hexagonal $YFe_{1-x}Pd_xO_{3-\delta}$: Nonperovskite host compounds for Pd^{2+} and their catalytic activity for CO oxidation, *Chemistry of Materials*, **2008**, *20*(20), 6567–6576.